NANO LETTERS
Letter
Cite This: Nano Lett. 2017, 17, 6935-6940
pubs.acs.org/NanoLett

Resolving the Spatial Structures of Bound Hole States in Black Phosphorus

Zhizhan Qiu,[†,‡] Hanyan Fang,[†] Alexandra Carvalho,[§] A. S. Rodin,[§] Yanpeng Liu,[†,§] Sherman J. R. Tan,[†,‡] Mykola Telychko,[†,§] Pin Lv,[†] Jie Su,[†,§] Yewu Wang,[⊥] A. H. Castro Neto,[§,∥] and Jiong Lu*[,†,§]

[†]Department of Chemistry, National University of Singapore, 3 Science Drive 3, Singapore 117543
[‡]NUS Graduate School for Integrative Sciences and Engineering, National University of Singapore, 28 Medical Drive, Singapore 117456
[§]Centre for Advanced 2D Materials and Graphene Research Centre, National University of Singapore, Singapore 117546
[∥]Department of Physics, National University of Singapore, 3 Science Drive 2, Singapore 117542
[⊥]Department of Physics & State Key Laboratory of Silicon Materials, Zhejiang University, Hangzhou 310027, P. R. China

Supporting Information

ABSTRACT: Understanding the local electronic properties of individual defects and dopants in black phosphorus (BP) is of great importance for both fundamental research and technological applications. Here, we employ low-temperature scanning tunnelling microscope (LT-STM) to probe the local electronic structures of single acceptors in BP. We demonstrate that the charge state of individual acceptors can be reversibly switched by controlling the tip-induced band bending. In addition, acceptor-related resonance features in the tunnelling spectra can be attributed to the formation of Rydberg-like bound hole states. The spatial mapping of the quantum bound states shows two distinct shapes evolving from an extended ellipse shape for the 1s ground state to a dumbbell shape for the $2p_x$ excited state. The wave functions of bound hole states can be well-described using the hydrogen-like model with anisotropic effective mass, corroborated by our theoretical calculations. Our findings not only provide new insight into the many-body interactions around single dopants in this anisotropic two-dimensional material but also pave the way to the design of novel quantum devices.

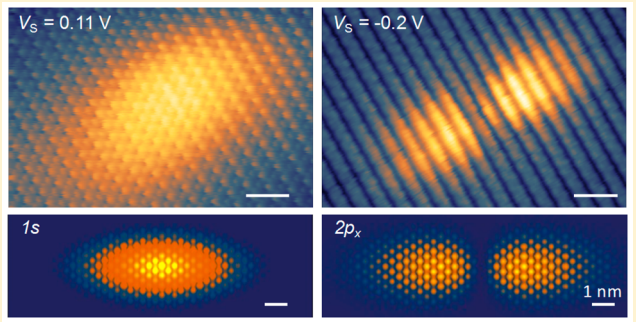

KEYWORDS: *Black phosphorus, Rydberg-like bound hole states, hydrogen-like model, charge state, scanning tunnelling microscopy*

Black phosphorus (BP), the most thermodynamically stable phosphorus allotrope, has emerged as a promising two-dimensional (2D) semiconductor owing to its widely tunable direct bandgap, high carrier mobility, and outstanding in-plane anisotropic properties.[1−4] The recent demonstrations of quantum oscillations, superconductivity, and electric field tunable bandgap in BP offer exciting prospects for applications in electronic and optoelectronic devices.[5−8] It is known that the native defects and impurities introduced during the synthesis and processing of BP have a profound impact on its physical properties and device characteristics.[9,10] For example, the p-type dominant transport behavior has frequently been observed in BP field effect transistor devices, presumably due to the donation of hole carriers from charge-active defects or absorbate.[2,11−13] It has also been predicted that electronically active defects and impurities could result in scattering-limited mobility anisotropy in BP, while the binding strength of the carriers to dopants in the host lattice has a significant influence on the charge transport properties of BP.[14,15] Hence, an atomic-level understanding of electronic properties surrounding the dopants and defects in BP is of prime importance for facilitating further optimization of its device characteristics. Despite remarkable research progress, microscopic defect and impurity physics in BP is far from being adequately understood. To this end, we performed a systematic LT-STM study to explore the quantum states of individual acceptors in BP and to probe their contributions to the local density of states. Our results reveal that the charge state of an individual shallow acceptor can be reversibly switched by using the STM tip. Furthermore, a hole bound to a negatively charged acceptor core leads to the formation of Rydberg-like bound states, manifesting in the tunnelling spectra acquired at acceptor sites. The acceptor-related resonances in the dI/dV spectra are associated with the ground and excited bound hole states. It is observed that the ground state is stretched along the armchair direction with a smaller effective carrier mass, giving rise to a peculiar ellipse shape in BP. In contrast, the excited state appears as a dumbbell-shaped feature consisting of two bright

Received: August 5, 2017
Revised: October 5, 2017
Published: October 16, 2017

DOI: 10.1021/acs.nanolett.7b03356
Nano Lett. 2017, 17, 6935−6940

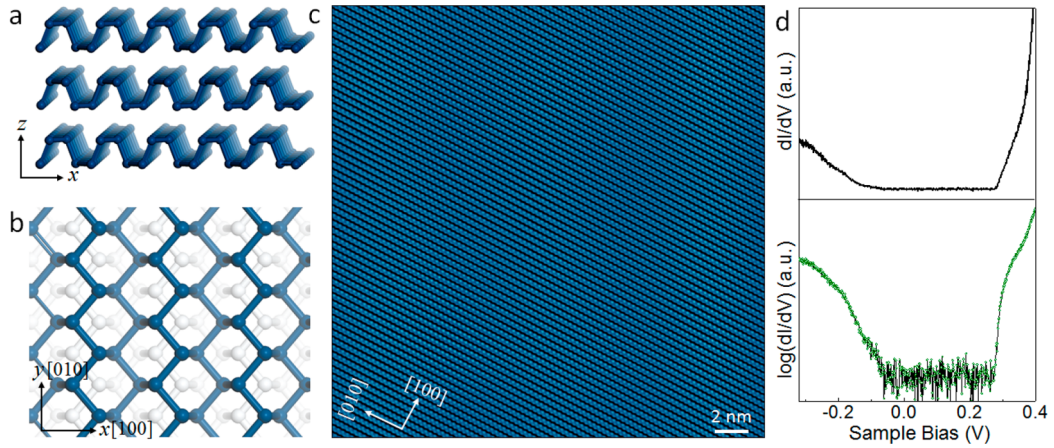

Figure 1. Probe the intrinsic doping of bare BP surface. (a,b) Sketches show the crystal structure of BP with the side view (a) and top view (b). The crystallographic directions are also labeled. (c) Atomically resolved STM image of bare BP regions free of defects (V_S = 0.3 V and I = 1 nA). The scale bar is 2 nm. (d) dI/dV data taken on clean BP region to probe the intrinsic doping (upper panel). The bottom panel shows the logarithm of dI/dV data for the precise determination of the band edges and band gap.

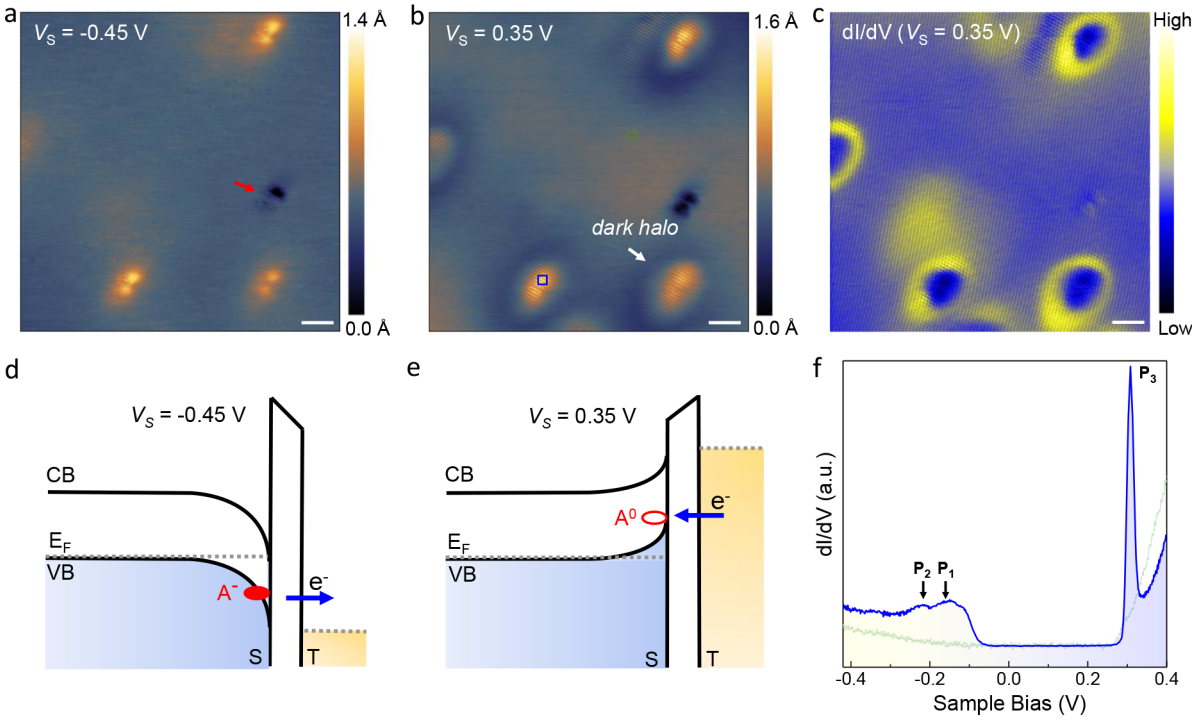

Figure 2. STM images and STS measurements of shallow acceptors in BP. (a,b) Typical 40 × 40 nm^2 constant-current STM image of acceptors in the cleaved BP sample taken at different sample biases: (a) V_S = −0.45 V and (b) V_S = 0.35 V. (c) Corresponding dI/dV mapping taken at V_S = 0.35 V. Scale bare is 4 nm. (d,e) Schematic illustration showing the switch of the charge state of the acceptor from the negatively charged state at V_S = −0.45 V (d) to the neutral state at V_S = 0.35 V. (e) through controlling the local tip induced band bending. (f) Local dI/dV spectra acquired at acceptor site (marked in a blue rectangle in b) and bare BP surface away from defect (marked in a green rectangle in b), corresponding to the blue and green dotted curves, respectively. Two weak resonances near the VB edge (P_1 and P_2) and a sharp feature (P_3) are resolved in the dI/dV spectra acquired at the acceptor site.

lobes and a dim center in the STM topographic image. The ellipse and dumbbell shapes observed in our experiment closely resemble the wave function patterns corresponding to the 1s and 2p$_x$ bound states modeled using a combination of analytical and numerical methods. The results presented here offer an atomic-level insight into the many-body interactions related to individual dopants in BP.

Unlike other 2D materials such as graphene and transition-metal dichalcogenides, BP undergoes rapid surface degradation under ambient conditions. In order to obtain the clean surface required for LT-STM studies of the acceptors in BP, we performed *in situ* exfoliation of bulk BP crystal along the [001] direction (marked in Figure 1a) in ultrahigh vacuum conditions to remove the degraded surface. After *in situ* cleavage, the sample was further heated to 550 K to remove potential surface adsorbates. Subsequently, we performed LT-STM measurement of the cleaved BP surface at 4.5 K using a tungsten tip calibrated spectroscopically against the Shockley surface state on Au(111) surface. Figure 1c shows the atomically resolved STM image of a clean surface region free of defects. The zigzag

DOI: 10.1021/acs.nanolett.7b03356
Nano Lett. 2017, 17, 6935−6940

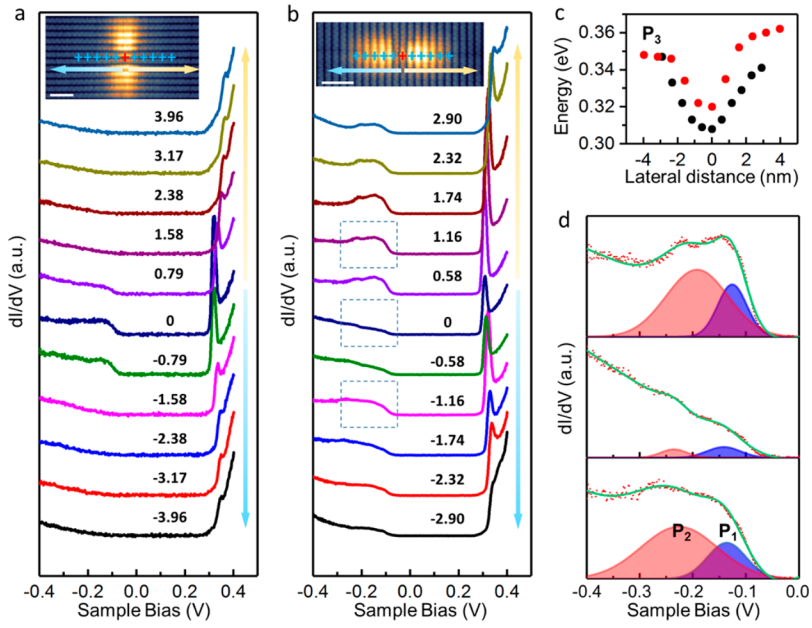

Figure 3. Spatially resolved dI/dV spectra near a charged acceptor in BP. (a,b) dI/dV spectra measured at different distances with respect to the center of individual acceptors along (a) zigzag direction and (b) armchair direction. Arrows indicate the direction away from the center of the acceptor. The scale bar in the inset figure is 2 nm. (c) Plot of the energy positions of peak P_3 versus the lateral distance of the tip (with respect to the center of acceptor) along zigzag (red dots) and armchair directions (black dots). (d) dI/dV spectra taken at 1.16 nm (upper panel), 0 nm (middle panel), and −1.16 nm (bottom panel) away from the center of the acceptor site (marked by dashed rectangle in b) were fitted to a sum of two Gaussian peaks as highlighted in blue (P_1) and red areas (P_2). The solid green line is the sum of fitted Gaussian peaks and a polynomial background. The red dotted line is the original dI/dV spectra.

rows along the [010] directions corresponding to the upper plane of atoms in the topmost puckered BP layer are clearly resolved (Figure 1b,c). A close look at atomic structures allows us to determine the lattice constant along the armchair (a = 4.4 ± 0.1 Å) and zigzag directions (b = 3.3 ± 0.1 Å), consistent with previous reports.[16−19] We also performed dI/dV spectroscopic measurements on the bare BP region to probe the intrinsic doping level of BP. The band edges are better determined by further conducting the logarithm of dI/dV curve shown in Figure 1d (black curve). Based on the logarithm dI/dV data (green curve in Figure 1d), the band gap of BP is determined to be 0.33 ± 0.02 eV, consistent with previous studies[7,19−21] (refer to Figure S1 for the detailed band gap determination). The valence band edge is located at −0.1 eV below the Fermi level (E_F), indicating an intrinsic p-doping effect presumably arising from unintentional acceptors in the cleaved BP sample. In a recent work, single vacancies are proposed as the source for p-doping in BP.[19] Our results, however, suggest that another possible hole doping source could be the Sn-related impurities introduced during the synthesis of the material. XPS elemental analysis reveals a noticeable signal from Sn impurities present in the top surface of cleaved BP (Figure S2). During the synthesis of BP, red phosphorus forms a molten alloy phase with Sn above the eutectic temperature. A subsequent cooling results in the precipitation of phosphorus from the liquid alloy to crystallize into BP structures.[22] It is most likely that a small portion of Sn atoms substitute P atoms in BP crystals, contributing to the intrinsic p-doping of BP. In addition, STM imaging of individual impurities near the surface reveals a protrusion feature at the center of the defect site (Figure S3), similar to previous observation of N-substitutional dopants in graphene.[23] Despite of the presence of different possibilities of p-type defects (either single vacancies or substitutional Sn dopant), our STM results show that the spatial structures of local quantum states created by individual acceptors are not dependent on the particular atomic arrangement of the atoms at the defect center, which will be further elaborated in detail later.

Figure 2a shows a representative 40 × 40 nm^2 STM image of several defects oriented in the [100] direction. A dark feature as indicated by the red arrow in Figure 2a is presumably associated with vacancy-related defect structures (refer to the Supporting Information S5 for details). The majority of the defects imaged here exhibit a dumbbell protrusion elongated along the armchair direction at both positive and negative sample biases. The density of these defects is estimated to (1.0 ± 0.3) × 10^{18} cm^{-3} by analyzing large-scale STM images as shown in Figure S5. A close examination of the STM image taken at a positive sample bias (Figure 2b) reveals that each bright dumbbell feature is surrounded by a dark halo structure, which turns into a brighter background surrounding the dumbbell protrusion at a negative sample bias (Figure 2a). Generally, the distinct dark halo structure arises from repulsive Coulombic interaction between the negatively charged center and electrons tunnelling into the empty states, while the brighter appearance surrounding the defect is due to the attractive interaction between the negatively charged defect and holes tunnelling into occupied states.[24] Hence, the contrast reversal observed here implies that the defects imaged are electrically active shallow acceptors, resembling the STM topographic contrast acquired around ionized dopants in conventional semiconductors.[24−26]

With this in mind, we now turn to the exploration of the electronic properties of individual acceptors by performing dI/dV measurements. In contrast to the featureless dI/dV curve taken on clean surface, the dI/dV spectrum (blue curve in Figure 2f) taken on individual acceptor sites (as marked by the blue square in Figure 2b) reveals two weak resonances at −0.13

DOI: 10.1021/acs.nanolett.7b03356
Nano Lett. 2017, 17, 6935−6940

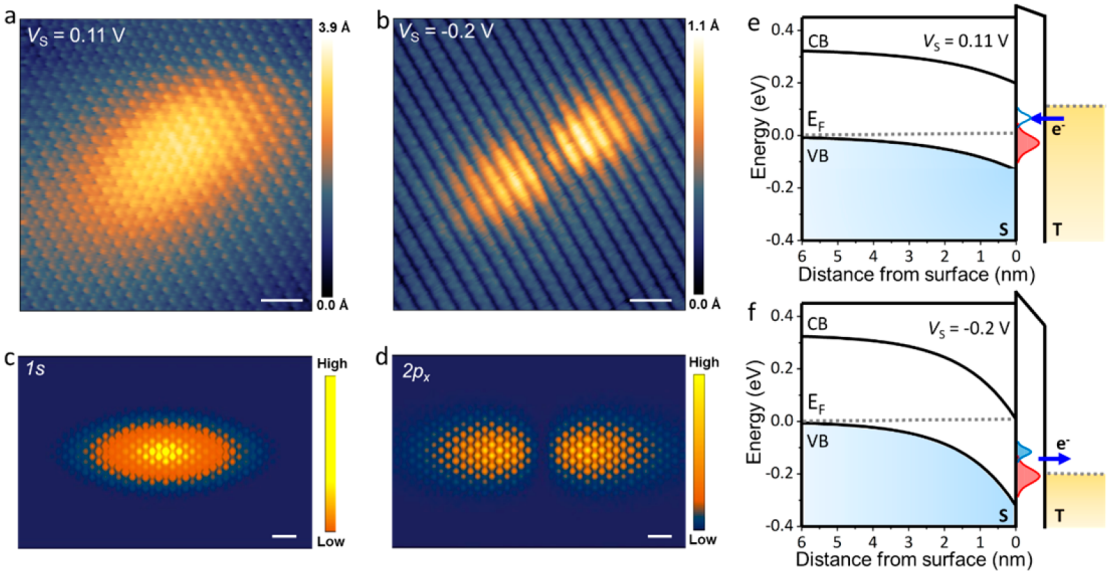

Figure 4. STM topographic images resolve the spatial structures of the bound hole states. (a) Ellipse shape for the ground state and (b) dumbbell shape for the excited state. (c,d) Top view of the squared wave function of 1s and 2p$_x$ states calculated using an anisotropic hydrogen-like model. (e,f) Schematic illustration of the occupation of bound states after taking the band bending into account: (e) P_1 is empty, and P_2 is filled at V_S = 0.11 V; (f) P_1 and P_2 states are filled at V_S = −0.2 V. Scale bar is 1 nm.

eV (P_1), −0.21 eV (P_2) and a sharp feature at 0.31 eV (P_3). As of now, the physical origin of the two weak features will tentatively be assigned to acceptor related states and will be further discussed in detail later. The observation of a sharp peak at positive sample bias (V_S = 0.31 V) signifies a tip-induced deionization of shallow acceptor states in BP. At the threshold voltage, tip-induced band bending shifts acceptor related states above E_F, resulting in deionization of the acceptor as illustrated in Figure 2e. The abrupt disappearance of the repulsive Coulomb interaction allows more electrons to tunnel into conduction band (CB) states that gives rise to a sharp feature in the dI/dV spectrum. Below the deionization voltage, acceptors are negatively charged. In particular, a strong downward band bending at a negative sample bias shifts the acceptor state further below E_F, facilitating the formation of stable negatively charged acceptor states as illustrated in Figure 2d. To further confirm this, we conducted the dI/dV mapping of the same spatial region at V_S = 0.35 V, slightly above the deionization voltage (V_S = 0.31 V). A striking ring-like feature enclosing each individual acceptor was clearly observed in the dI/dV map (Figure 2c). This observation further indicates at a specific sample bias above 0.31 V the acceptor is deionized due to the hole occupation of acceptor states when the tip is held inside the ring, whereas the acceptor is ionized due to electron occupation of acceptor states when the tip is outside the ring. Such a tip-induced charging ring has been previously seen in different physical systems.[25−30] Hence, the charge states of individual acceptors can be reversibly switched using a STM tip via the manipulation of bias voltages or tip positions.

To better understand the electronic structures surrounding the individual acceptors, we conducted spatially resolved dI/dV spectroscopic measurement across the center of acceptor site along the zigzag and armchair directions as shown in Figure 3a,b. It is expected that the threshold voltage required to switch the charge state of individual acceptors will be gradually reduced to the minimum as the tip laterally approaches the center of the defect.[26] Indeed, a plot of the energy position of P_3 versus the lateral distance of the tip (with respect to the center of the acceptor) along zigzag and armchair directions shows that P_3 shifts toward E_F and reaches the energy minimum at the center of the acceptor (Figure 3c), which further proves that this peak originates from tip-induced deionization. Having understood the origin of the deionization peak (P_3), we now begin to explore the spatial variation of two acceptor-related weak resonances (P_1 and P_2). It is found that along the zigzag direction these two peaks undergo a fast spatial decay and vanish at a distance of around 0.8 nm away from the center of defects (Figure 3a). In contrast, these features show a much larger spatial extension over a diameter of more than 6 nm along the armchair direction (Figure 3b). To our surprise, the maximum local density of states (LDOS) of acceptor-related states was observed at a distance of ±1.16 nm (as marked in Figure 3b) away from the center of acceptor sites, coinciding with the center of individual bright lobes in the STM topographic image (inset of Figure 3b). To extract the experimental energies and peak intensity of these electronic states, we fit dI/dV spectra taken at three representative sites (at the center and at a distance of ±1.16 nm away from center of acceptor) to a sum of two Gaussian peaks with a polynomial function as the background. The energies of P_1 and P_2 is determined to be −0.13 ± 0.01 and −0.21 ± 0.02 eV, respectively, as shown in Figure 3d.

These spectroscopic features observed near the acceptor sites can be explained within a general shallow dopant physics framework. Each carrier interacts with its negatively charged acceptor center in analogy to the hydrogen atom model, leading to the formation of Rydberg-like bound hole states.[31,32] Indeed, the spatially extended dumbbell feature observed here resembles the anisotropic bound states near individual acceptors in conventional III−V semiconductors,[25,27,32] suggesting the formation of bound hole states around acceptors in BP. Hence, P_1 and P_2 can be interpreted as the ground state and the excited state, respectively. By performing bias-dependent STM imaging, we managed to resolve two distinct structures, which can be attributed to the ground and excited bound states. As shown in Figure 4b, a dumbbell shape was

DOI: 10.1021/acs.nanolett.7b03356
Nano Lett. 2017, 17, 6935−6940

clearly imaged around the negatively charged acceptor at V_S = −0.2 V. As we increase the sample bias up to 0.11 V, the dumbbell shape transforms into an ellipse shape, which eventually reverts back to the original dumbbell-shape at sample bias above 0.31 V, where the acceptor is now at the neutral state (Figure S7). To better interpret our data, the tip-induced local band bending effect needs to be taken into account. We estimated the tip induced band bending (TIBB) by solving the one-dimensional Poisson equation as described in the previous report.[33] Based on our TIBB calculation (refer to Supporting Information S7 for details), the ground state (P_1) is empty, but the excited state (P_2) is filled at V_S = 0.11 V as illustrated in Figure 4e. Hence, the ground state dominates the tunnelling process at V_S = 0.11 V and exhibits an ellipse shape in the STM image. At a sample bias of −0.2 V, the excited state (P_2) dominates the tunnelling process with a negligible contribution from the ground state (P_1) due to its weaker LDOS (illustrated in Figure 4f). As a result, the dumbbell shape observed around the charged acceptor can be attributed to the excited hole state. We also managed to resolve the dumbbell feature for the acceptor at the neutral state at V_S = 0.35 V (Figure S7). Our results indicate that the dumbbell-shape arises from the intrinsic wave function of the excited bound state rather than from the screened Coulomb potential induced band bending near the ionized acceptor.

To further elucidate the nature of these electronic states, we first simulated the STM image of the phosphorene valence band state and the negatively charged shallow acceptors (either single vacancies or substitutional Sn dopant) using density functional theory (Figure S8). Based on the calculated results, we conclude that spatial structures presented in Figure 4a,b cannot be obtained from the noninteracting electron system alone, but only if the Coulomb interaction of the hole with the negatively charged acceptor center and the respective hydrogen-like states are taken into account. Hence, we performed theoretical modeling of bound hole states using a hydrogen-like model with the anisotropic effective mass. The solution of the anisotropic hydrogen model in 2D is nontrivial, and therefore, we introduce a few approximations. Our first assumption is that the hole wave function is localized in the top layer of BP, reducing our problem to two-dimensional in nature. In addition, we assume that the permittivity of the medium is isotropic and is equal to the geometric average of the permittivities in two dimensions.[34] The anisotropic hydrogen-like equation can be solved using the numerical method presented in previous work.[35] Using this approach, we obtain the approximate wave functions for the 1s, 2s, $2p_y$, and $2p_x$ states. As shown in Figure 4c,d, both the 1s and $2p_x$ states are oriented along the armchair direction, whereas the 2s and $2p_y$ states are oriented along the zigzag direction (Figure S9). A close examination of the nodal structures and orientations of calculated wave functions allows us to assign the ground state (P_1) and the excited state (P_2) observed in our experiment to the 1s state and $2p_x$ state, respectively. As expected, 1s ground state is strongly extended along the armchair direction with smaller effective mass, consistent with the spatial structures of the ground state of excitons predicted in monolayer and few-layer black phosphorus.[4,35−37] Compared to a monolayer, the states in few-layer systems experience reduced screening, leading to weaker localization and smaller separation between the energy levels. The degeneracy of excited states (2s, $2p_y$, and $2p_x$) with the same primary quantum number but different azimuthal quantum numbers can be broken arising from the anisotropy of the band mass along zigzag and armchair directions.[38] The exact energy ordering of the excited states (2s, $2p_y$, and $2p_x$) strongly depends on screening and the carrier masses in such highly anisotropic system. It has been predicted that the 2s state lies above 2p states in this system.[38] Hence, it is most likely that the tunneling current contributed from the high energy valence band states is dominant over 2s state, making it challenging to resolve the spatial structure of the 2s state in the STM image. The absence of $2p_y$ is presumably due to its weak LDOS arising from an ineffective coupling with valence band edge states (refer to Supporting Information S9 for details). Although we have made considerable approximations concerning all these factors, our numerical results are in good agreement with the experimental results.

In summary, we have demonstrated a controllable charge switch of individual acceptors in BP by manipulating the local tip gating effect. Our results show that the acceptor-related features in the dI/dV spectra can be associated with the ground and excited bound hole states. We also directly discovered that the spatial shape of bound states evolve from an extended ellipse shape for the ground state to a dumbbell shape for the excited state. The physical origin of the anisotropic shape of bound states can be well-described using the anisotropic hydrogenic model. We expect that our findings provide a generic picture for describing the spatial structural and electronic properties of bound states near shallow dopants in BP, opening avenues for the development of novel quantum devices using many-body states in this anisotropic 2D semiconducting crystal.

■ ASSOCIATED CONTENT

Supporting Information

The Supporting Information is available free of charge on the ACS Publications website at DOI: 10.1021/acs.nanolett.7b03356.

Details of the experiment and theory method, electronic band gap determination, XPS data collected on as-exfoliated BP, STM image of the acceptor near the surface, vacancy related defects, probing the density of defects, evaluation of tip-induced band bending, spatial mapping of the acceptor at neutral state, constant-current STM images modeled for negative shallow acceptors in BP, and squared wave functions of bound hole states (PDF)

■ AUTHOR INFORMATION

Corresponding Author

*E-mail: chmluj@nus.edu.sg.

ORCID

Sherman J. R. Tan: 0000-0003-1591-3497

Jiong Lu: 0000-0002-3690-8235

Author Contributions

Z.Q. and H.F. contributed equally to this work. J.L. conceived and supervised the project. Z.Q. performed the STM imaging and STS measurement. Z.Q. and H.F. carried out the STS analysis and band bending calculations. Y.L., M.T., and P.L. helped with STM characterization. S.J.R.T. and Y.L. performed XPS measurement. A.C., A.R., and A.H.C.N. contributed to the theoretical calculations. Z.Q. and J.L. wrote the paper with the contribution from A.C. and S.J.R.T. All authors took part in the discussion and preparation of the manuscript.

DOI: 10.1021/acs.nanolett.7b03356
Nano Lett. 2017, 17, 6935−6940

Notes

The authors declare no competing financial interest.

■ ACKNOWLEDGMENTS

J. Lu acknowledge the support from NUS start-up grant (R-143-000-621-133) and Tier 1 (R-143-000-637-112) and MOE Tier 2 grant (R-143-000-682-112). The first-principles calculations were carried out on the Centre for Advanced 2D Materials computing facilities.

■ REFERENCES

(1) Li, L.; Kim, J.; Jin, C.; Ye, G. J.; Qiu, D. Y.; da Jornada, F. H.; Shi, Z.; Chen, L.; Zhang, Z.; Yang, F.; Watanabe, K.; Taniguchi, T.; Ren, W.; Louie, S. G.; Chen, X. H.; Zhang, Y.; Wang, F. *Nat. Nanotechnol.* **2017**, *12*, 21−25.
(2) Tran, V.; Soklaski, R.; Liang, Y.; Yang, L. *Phys. Rev. B: Condens. Matter Mater. Phys.* **2014**, *89* (23), 235319.
(3) Xia, F.; Wang, H.; Jia, Y. *Nat. Commun.* **2014**, *5*, 4458.
(4) Wang, X.; Jones, A. M.; Seyler, K. L.; Tran, V.; Jia, Y.; Zhao, H.; Wang, H.; Yang, L.; Xu, X.; Xia, F. *Nat. Nanotechnol.* **2015**, *10*, 517−521.
(5) Li, L.; Ye, G. J.; Tran, V.; Fei, R.; Chen, G.; Wang, H.; Wang, J.; Watanabe, K.; Taniguchi, T.; Yang, L. *Nat. Nanotechnol.* **2015**, *10*, 608−613.
(6) Deng, B.; Tran, V.; Xie, Y.; Jiang, H.; Li, C.; Guo, Q.; Wang, X.; Tian, H.; Koester, S. J.; Wang, H. *Nat. Commun.* **2017**, *8*, 14474.
(7) Liu, Y.; Qiu, Z.; Carvalho, A.; Bao, Y.; Xu, H.; Tan, S. J.; Liu, W.; Castro Neto, A.; Loh, K. P.; Lu, J. *Nano Lett.* **2017**, *17*, 1970−1977.
(8) Zhang, R.; Waters, J.; Geim, A. K.; Grigorieva, I. V. *Nat. Commun.* **2017**, *8*, 15036.
(9) Ebert, H. P. *Mater. Today* **2003**, *6*, 36−43.
(10) Koenraad, P. M.; Flatte, M. E. *Nat. Mater.* **2011**, *10*, 91−100.
(11) Doganov, R. A.; O'Farrell, E. C.; Koenig, S. P.; Yeo, Y.; Ziletti, A.; Carvalho, A.; Campbell, D. K.; Coker, D. F.; Watanabe, K.; Taniguchi, T. *Nat. Commun.* **2015**, *6*, 6647.
(12) Han, C.; Hu, Z.; Carvalho, A.; Guo, N.; Zhang, J.; Hu, F.; Xiang, D.; Wu, J.; Lei, B.; Wang, L. *2D Mater.* **2017**, *4*, 021007.
(13) Koenig, S. P.; Doganov, R. A.; Schmidt, H.; Neto, A. H. C.; Özyilmaz, B. *Appl. Phys. Lett.* **2014**, *104*, 103106.
(14) Zou, Y.-L.; Song, J.; Bai, C.; Chang, K. *Phys. Rev. B: Condens. Matter Mater. Phys.* **2016**, *94*, 035431.
(15) Liu, Y.; Low, T.; Ruden, P. P. *Phys. Rev. B: Condens. Matter Mater. Phys.* **2016**, *93*, 165402.
(16) Qiao, J.; Kong, X.; Hu, Z.-X.; Yang, F.; Ji, W. *Nat. Commun.* **2014**, *5*, 4475.
(17) Low, T.; Rodin, A.; Carvalho, A.; Jiang, Y.; Wang, H.; Xia, F.; Neto, A. C. *Phys. Rev. B: Condens. Matter Mater. Phys.* **2014**, *90*, 075434.
(18) Liang, L.; Wang, J.; Lin, W.; Sumpter, B. G.; Meunier, V.; Pan, M. *Nano Lett.* **2014**, *14*, 6400−6406.
(19) Kiraly, B.; Hauptmann, N.; Rudenko, A.; Katsnelson, M. I.; Khajetoorians, A. A. *Nano Lett.* **2017**, *17*, 3607−3612.
(20) Morita, A. *Appl. Phys. A: Solids Surf.* **1986**, *39*, 227−242.
(21) Akahama, Y.; Endo, S.; Narita, S.-i. *J. Phys. Soc. Jpn.* **1983**, *52*, 2148−2155.
(22) Zhao, M.; Niu, X.; Guan, L.; Qian, H.; Wang, W.; Sha, J.; Wang, Y. *CrystEngComm* **2016**, *18*, 7737−7744.
(23) Zhao, L.; He, R.; Rim, K. T.; Schiros, T.; Kim, K. S.; Zhou, H.; Gutiérrez, C.; Chockalingam, S.; Arguello, C. J.; Pálová, L. *Science* **2011**, *333*, 999−1003.
(24) Feenstra, R. M.; Meyer, G.; Moresco, F.; Rieder, K. *Phys. Rev. B: Condens. Matter Mater. Phys.* **2002**, *66*, 165204.
(25) Yakunin, A.; Silov, A. Y.; Koenraad, P.; Wolter, J.; Van Roy, W.; De Boeck, J.; Tang, J.-M.; Flatté, M. *Phys. Rev. Lett.* **2004**, *92*, 216806.
(26) Teichmann, K.; Wenderoth, M.; Loth, S.; Ulbrich, R.; Garleff, J.; Wijnheijmer, A.; Koenraad, P. *Phys. Rev. Lett.* **2008**, *101*, 076103.
(27) Marczinowski, F.; Wiebe, J.; Tang, J.-M.; Flatté, M.; Meier, F.; Morgenstern, M.; Wiesendanger, R. *Phys. Rev. Lett.* **2007**, *99*, 157202.
(28) Wong, D.; Velasco, J., Jr; Ju, L.; Lee, J.; Kahn, S.; Tsai, H.-Z.; Germany, C.; Taniguchi, T.; Watanabe, K.; Zettl, A. *Nat. Nanotechnol.* **2015**, *10*, 949−953.
(29) Wickenburg, S.; Lu, J.; Lischner, J.; Tsai, H.-Z.; Omrani, A. A.; Riss, A.; Karrasch, C.; Bradley, A.; Jung, H. S.; Khajeh, R.; Wong, D.; Watanabe, K.; Taniguchi, T.; Zettl, A.; Neto, A. H. C.; Louie, S. G.; Crommie, M. F. *Nat. Commun.* **2016**, *7*, 13553.
(30) Brar, V. W.; Decker, R.; Solowan, H.-M.; Wang, Y.; Maserati, L.; Chan, K. T.; Lee, H.; Girit, C. O.; Zettl, A.; Louie, S. G.; Cohen, M. L.; Crommie, M. F. *Nat. Phys.* **2011**, *7*, 43−47.
(31) Schubert, E. F. *Doping in III-V Semiconductors*; Cambridge University Press: Cambridge, 2015.
(32) Mahieu, G.; Grandidier, B.; Deresmes, D.; Nys, J.; Stiévenard, D.; Ebert, P. *Phys. Rev. Lett.* **2005**, *94*, 026407.
(33) Seiwatz, R.; Green, M. *J. Appl. Phys.* **1958**, *29*, 1034−1040.
(34) Nagahama, T.; Kobayashi, M.; Akahama, Y.; Endo, S.; Narita, S.-i. *J. Phys. Soc. Jpn.* **1985**, *54*, 2096−2099.
(35) Rodin, A.; Carvalho, A.; Neto, A. C. *Phys. Rev. B: Condens. Matter Mater. Phys.* **2014**, *90*, 075429.
(36) Tran, V.; Soklaski, R.; Liang, Y. F.; Yang, L. *Phys. Rev. B: Condens. Matter Mater. Phys.* **2014**, *89*, 89.
(37) Tran, V.; Fei, R. X.; Yang, L. *2D Mater.* **2015**, *2*, 044014.
(38) Qiu, D. Y.; da Jornada, F. H.; Louie, S. G. *Nano Lett.* **2017**, *17*, 4706−4712.

DOI: 10.1021/acs.nanolett.7b03356
Nano Lett. 2017, 17, 6935−6940